Supplement of Atmos. Chem. Phys., 26, 7081–7103, 2026
https://doi.org/10.5194/acp-26-7081-2026-supplement

Atmospheric Chemistry and Physics
Open Access
EGU

Supplement of

Long-term ozone formation sensitivity in China: spatiotemporal evolution and machine learning attribution

Jinglan Lin et al.

Correspondence to: Weihua Chen (chenwh26@jnu.edu.cn)

Table S1. Comparison of the FNR threshold ranges for the five city clusters during the warm season (April–September 2005–2023) derived in this study and reported in previous studies. Values in brackets indicate the threshold ranges.

Region	FNR threshold ranges			Threshold Range	Studied period	Reference	Spatial Coverage
	Scenarios 1 (S1[1])	Scenario 2 (S2[2])	Scenario 3 (S3[3])				
BTH	2.33[1.51, 3.30]	[1.00, 5.10]	[1.92, 2.85]	[2.0, 3.1]	Apr.–Sep. 2019–2022	BTH	Song et al., 2023
				[4.0, 5.1]	May–Oct. 2018–2022	Jing-Jin-Ji-Lu-Yu (JJJLY)	Li et al., 2024
				[3.0, 3.8]	Apr.–Sep. 2019–2021	Beijing-Tianjin-Hebei-Shandong	Ren et al., 2022
				[1.142, 2.268]	May–Nov. 2016–2018	North China (NC)	Du et al., 2022
				[1.2, 2.0]	Apr.–Oct. 2013–2014	BTH	Zhang et al., 2024
				[1.1, 1.9]	Apr.–Oct. 2015–2016		
				[1.0, 1.8]	Apr.–Oct. 2017–2019		
FWP	3.42[2.26, 4.77]	[1.14, 4.30]	[1.96, 3.19]	[1.142, 2.268]	May–Nov. 2016–2018	North China (NC)	Du et al., 2022
				[1.524, 3.001]	May–Nov. 2016–2018	Northwest China (NWC)	Du et al., 2022
				[3.2, 4.3]	Apr.–Sep. 2019–2021	Shanxi-Shaanxi-Henan	Ren et al., 2022

				[2.9, 4.0]	May–Oct. 2018–2022	Jiang-Zhe-Hu-Wan (JZHW)	Li et al., 2024
				[2.2, 3.3]	Apr.–Sep. 2019–2021	Shanghai-Jiangsu-Zhejiang-Anhui	Ren et al., 2022
YRD	1.59[0.90, 2.37]	[1.00, 4.00]	[1.72, 2.64]	[1.3, 2.1]	Apr.–Oct. 2013–2014		
				[1.2, 2.0]	Apr.–Oct. 2015–2016	YRD	Zhang et al., 2024
				[1.0, 1.8]	Apr.–Oct. 2017–2019		
				[3.1, 4.2]	May–Oct. 2018–2022	Chuan-Yu (CY)	Li et al., 2024
				[0.887, 2.479]	May–Nov. 2016–2018	Southwest China (SWC)	Du et al., 2022
				[2.5, 4.3]	Apr.–Sep. 2019–2021	Sichuan-Chongqing-Guizhou-Yunnan	Ren et al., 2022
SCB	3.24[1.93, 4.73]	[0.89, 4.30]	[1.70, 2.85]	[1.4, 2,2]	Apr.–Oct. 2013–2014		
				[1.2, 2.0]	Apr.–Oct. 2015–2016	Chuan-Yu (CY)	Zhang et al., 2024
				[1.1, 1.9]	Apr.–Oct. 2017–2019		
				[2.3, 3.4]	May–Oct. 2018–2022	Guangdong-Hong Kong-Macao-Guangxi-Hainan	Li et al., 2024
				[1.041, 3.068]	May–Nov. 2016–2018	South China (SC)	Du et al., 2022
PRD	2.62[1.66, 3.70]	[1.04, 3.80]	[2.02, 3.13]	[2.7, 3.8]	Apr.–Sep. 2019–2021	Guangdong-Hong Kong-Macao-Guangxi-Hainan	Ren et al., 2022
				[2.4, 3.2]	Apr.–Oct. 2013–2014		
				[2.0, 2.8]	Apr.–Oct. 2015–2016	Guangdong	Zhang et al., 2024
				[1.7, 2.5]	Apr.–Oct.		

					2017–2019		
China	2.02[1.20, 2.97]	[1.65, 4.20]	[2.03, 3.51]	[2.3, 4.2]	May–Oct. 2016–2019	China	Wang et al., 2021
				[2.2, 3.2]	Apr.–Sep. 2019–2021	China	Ren et al., 2022
				[1.92, 3.77]	Jun.–Aug. 2023	China	Fan et al., 2025
				[2.10, 3.87]	Sep.–Nov. 2023	China	Fan et al., 2025
				[1.64, 2.52]	May–Nov. 2016–2018	China	Du et al., 2022
ORC	2.07[1.17, 3.08]	/	/	/	/	/	/

[1] S1 denotes the region-specific thresholds derived in this study. [2] S2 denotes the minimum–maximum threshold ranges compiled from previous studies. [3] S3 denotes the averaged threshold ranges based on the corresponding minimum and maximum values.

Table S2. Mann–Kendall trend test and Sen's slope estimate for HCHO, NO_2, and FNR in the five major urban agglomerations in China during the warm season (April–September) from 2005 to 2023.

Variable	Region	Sen's slope	MK p-value	Pettitt's change point	Pettitt's p-value
NO_2[a]	BTH	-0.23	< 0.05	2015	< 0.05
	FWP	-0.09	< 0.05	2014	< 0.05
	YRD	-0.14	< 0.05	2014	< 0.05
	SCB	-0.01	> 0.05	2008	> 0.05
	PRD	-0.20	< 0.05	2014	< 0.05
HCHO[a]	BTH	0.15	< 0.05	2013	< 0.05
	FWP	0.12	< 0.05	2015	< 0.05
	YRD	0.12	< 0.05	2015	< 0.05
	SCB	0.09	< 0.05	2017	< 0.05
	PRD	0.06	< 0.05	2015	> 0.05
FNR[b]	BTH	0.06	< 0.05	2014	< 0.05
	FWP	0.06	< 0.05	2013	< 0.05
	YRD	0.04	< 0.05	2013	< 0.05
	SCB	0.00	< 0.05	2017	> 0.05
	PRD	0.06	> 0.05	2014	< 0.05

[a] HCHO and NO_2 are reported in units of $\times 10^{15}$ molec cm^{-2}. [b] FNR is dimensionless.

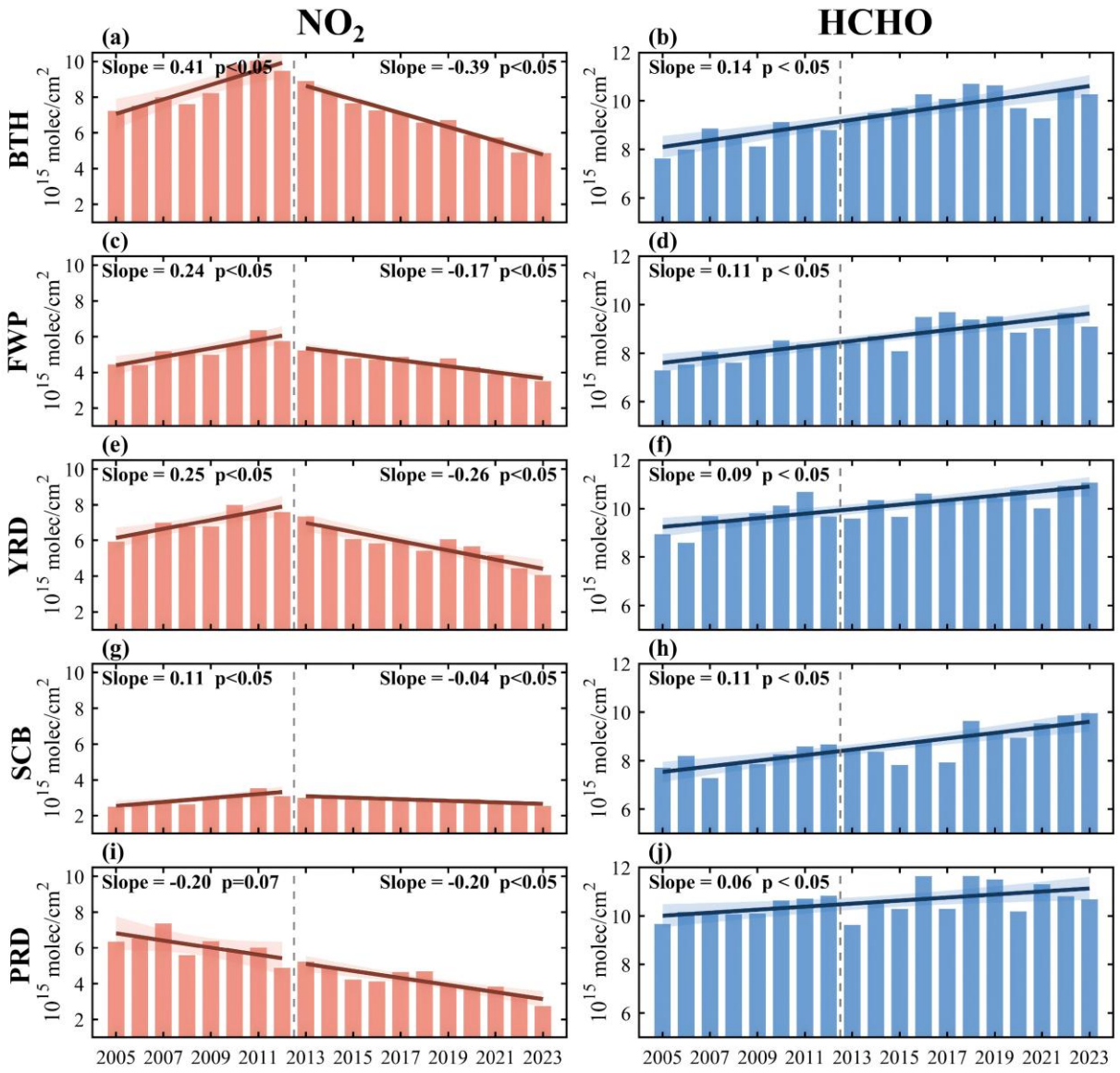

Figure S1. Interannual variations of NO_2 and HCHO column density in five key regions of China during the warm season (April–September) from 2005 to 2023.

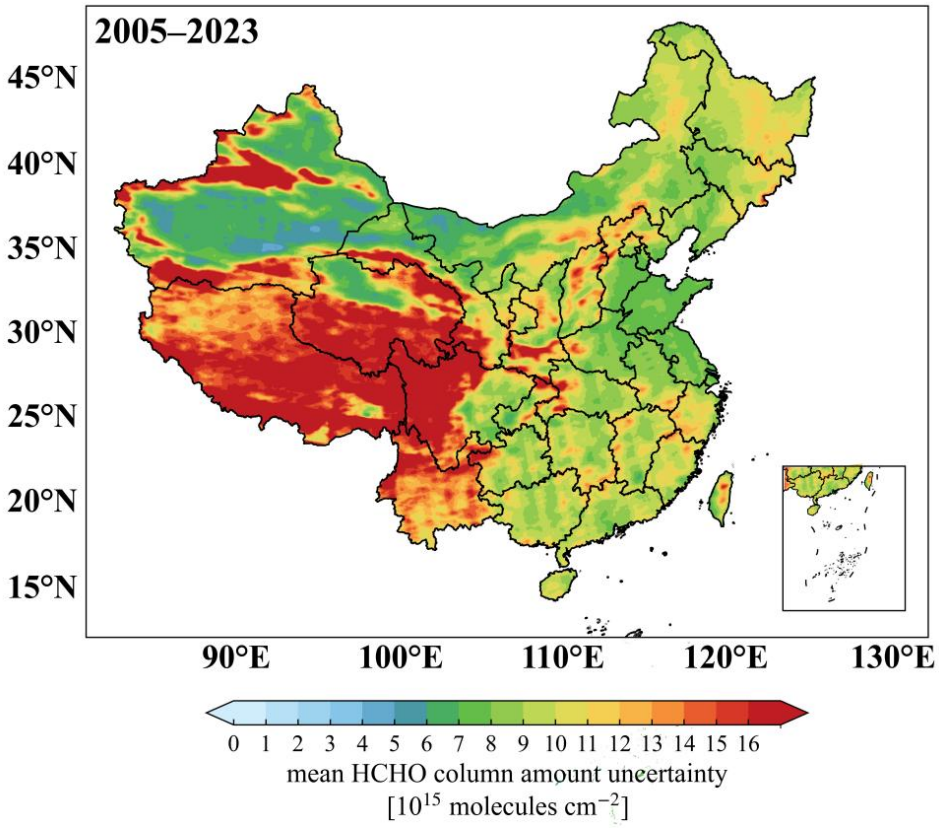

Figure S2. Uncertainty of the mean HCHO column over China during the warm season (April–September) from 2005 to 2023.

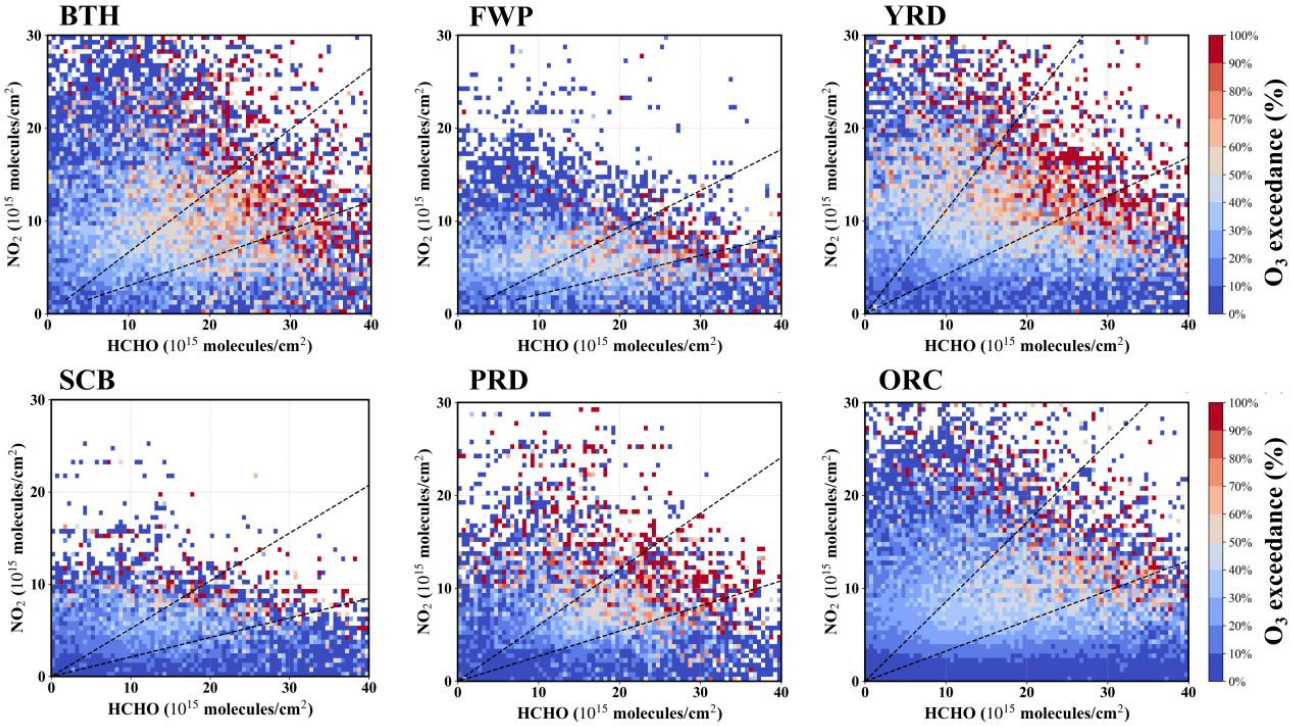

Figure S3. O_3 exceedance probability as a function of OMI HCHO and NO_2 for the six regions during the warm season (April–September) from 2015 to 2023. The black dashed lines indicate the OMI HCHO/NO_2 values corresponding to the derived FNR threshold ranges used to classify NO_x-limited, transitional, and VOC-limited regimes.

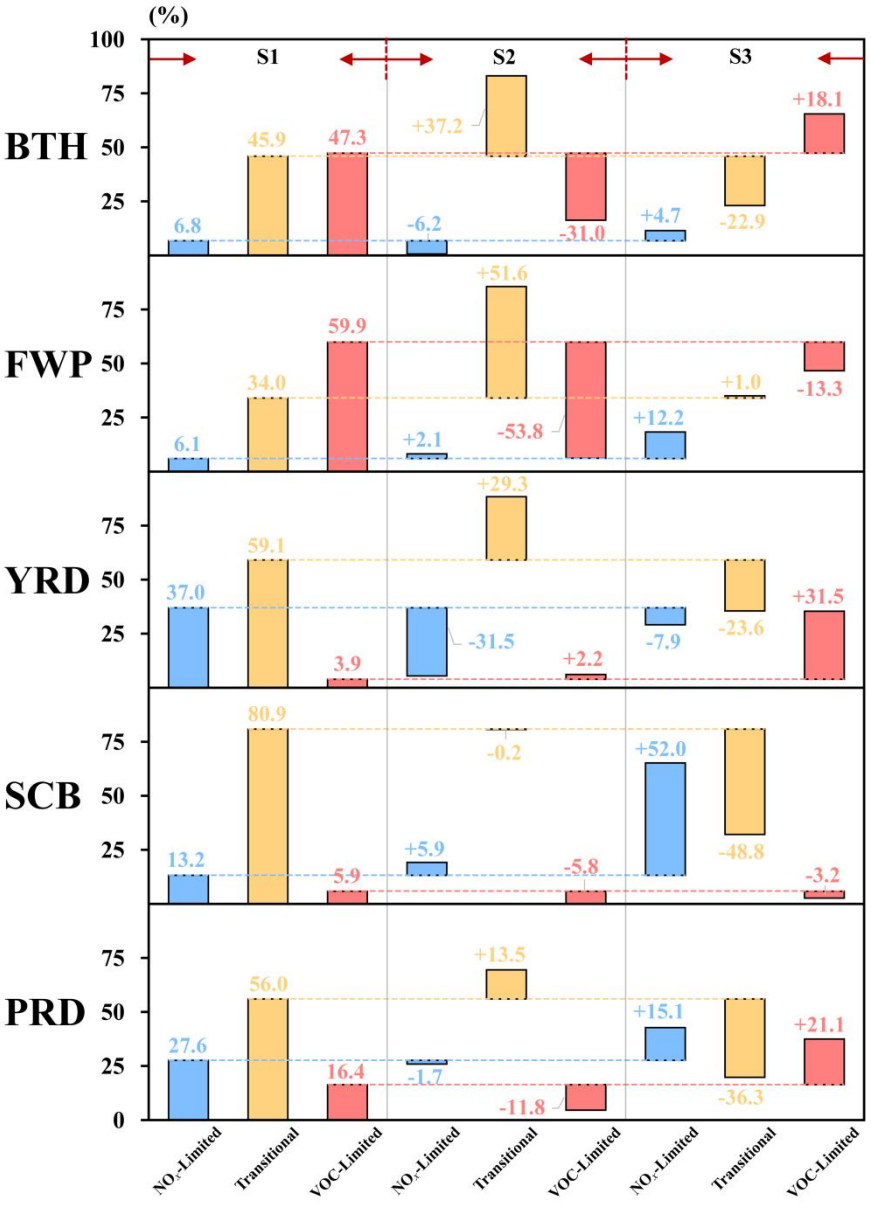

Figure S4. Sensitivity of OFS regime area fractions to different FNR threshold scenarios in the five major city clusters during the warm season (April–September) over 2005–2023. S1 denotes the region-specific thresholds derived in this study, S2 denotes the minimum–maximum threshold ranges compiled from previous studies, and S3 denotes the averaged threshold ranges based on the corresponding minimum and maximum values. Bars represent deviations in regime area fractions under S2 and S3 relative to S1.

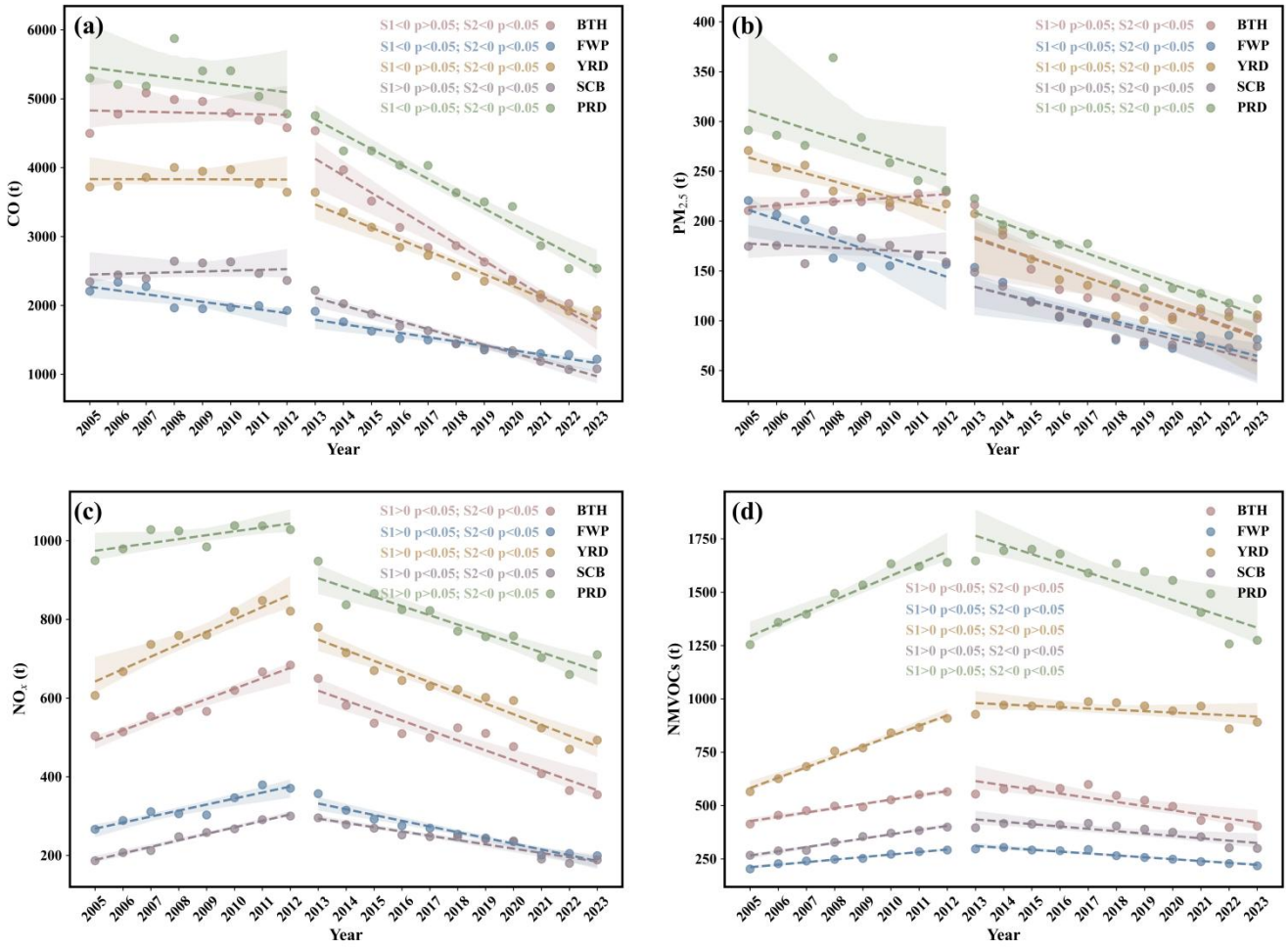

Figure S5. Interannual variations in warm-season (April–September) mean anthropogenic emissions of (a) CO, (b) $PM_{2.5}$, (c) NO_x, and (d) NMVOCs in the five city clusters from 2005 to 2023. Dots represent the annual mean values, dashed lines indicate the linear trends, and shaded areas show the 95% confidence intervals.

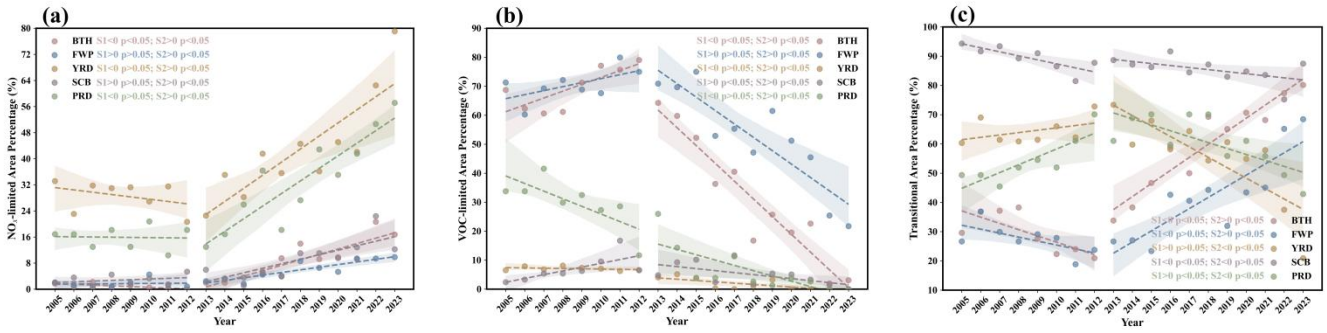

Figure S6. Interannual variations in warm-season (April–September) mean area fractions of (a) NO_x-limited, (b) VOC-limited and (c) transitional regimes in the five city clusters from 2005 to 2023. Dots represent the annual mean values, dashed lines indicate the linear trends, and shaded areas show the 95% confidence intervals.

Reference

Du, X., Tang, W., Cheng, M., Zhang, Z., Li, Y., Li, Y., and Meng, F.: Modeling of spatial and temporal variations of ozone-NO_x-VOC sensitivity based on photochemical indicators in China, J. Environ. Sci., 114, 454–464, https://doi.org/10.1016/j.jes.2021.12.026, 2022.

Fan, J., Yu, C., Li, Y., Zhang, Y., Fan, M., Tao, J., and Chen, L.: Comparison of FNR and GNR Based on TROPOMI Satellite Data for Ozone Sensitivity Analysis in Chinese Urban Agglomerations, Remote Sens., 17, 3321, https://doi.org/10.3390/rs17193321, 2025.

Li, Y., Yu, C., Tao, J., Lu, X., and Chen, L.: Analysis of Ozone Formation Sensitivity in Chinese Representative Regions Using Satellite and Ground-Based Data, Remote Sens., 16, 316, https://doi.org/10.3390/rs16020316, 2024.

Ren, J., Guo, F., and Xie, S.: Diagnosing ozone–NO_x–VOC sensitivity and revealing causes of ozone increases in China based on 2013–2021 satellite retrievals, Atmos. Chem. Phys., 22, 15035–15047, https://doi.org/10.5194/acp-22-15035-2022, 2022.

Song, H., Zhao, W., Yang, X., Hou, W., Chen, L., and Ma, P.: Ozone Sensitivity Analysis and Ozone Formation Regimes Division in the Beijing–Tianjin–Hebei Region Based on Satellite Remote Sensing Data, Atmosphere, 14, 1637, https://doi.org/10.3390/atmos14111637, 2023.

Wang, W., van der A, R., Ding, J., van Weele, M., and Cheng, T.: Spatial and temporal changes of the ozone sensitivity in China based on satellite and ground-based observations, Atmos. Chem. Phys., 21, 7253–7269, https://doi.org/10.5194/acp-21-7253-2021, 2021.

Zhang, J., Shen, A., Jin, Y., Cui, Y., Xu, Y., Lu, X., Liu, Y., and Fan, Q.: Evolution of ozone formation regimes during different periods in representative regions of China, Atmos. Environ., 338, 120830, https://doi.org/10.1016/j.atmosenv.2024.120830, 2024.